Supporting Information of

Synergistic and Autocatalytic Proton Shuttle with a Bifunctional Solid Acid in Low-Toxic Molten Salt Hydrate for Efficient Levulinic Acid Production from Cellulose

Zhenbang Liu[a,b], Shenghui Zhou[b], Jiangang Wang[c], Jinghua Wang [a, b]*, Hongyou Cui [b]*

a College of Chemistry, Chemical Engineering and Materials Science, Zaozhuang University, Zaozhuang, 277160, China;

b School of Chemistry and Chemical Engineering, Shandong University of Technology, Zibo 255000, China;

c School of Materials and Chemical Engineering, Zibo Polytechnic University, Zibo 255000, China.

E-mail: wangjh720422@126.com, cuihy@sdut.edu.cn

Table S1 Element content by EDS

	Elements, %					Si/Al	P/Nb
	O	Al	Si	P	Nb		
HZSM-5	67.22	1.82	30.74	-	-	16.89	-
Nb_2O_5/HZSM-5	63.61	1.37	34.11	-	0.91	24.90	-
Nb-P/HZSM-5	65.85	1.39	28.83	3.37	0.56	20.74	6.0

EDS analysis demonstrates the successful introduction of Nb and P species during the catalyst modification, accompanied by corresponding variations in the elemental composition and the Si/Al ratio.

Table S2 Elemental composition analysis of catalyst by XRF

Catalyst	Mass, %				Si/Al	Nb/P
	Al_2O_3	SiO_2	P_2O_5	Nb_2O_5		
HZSM-5	4.09	95.1	-	-	19.73	
Nb_2O_5/HZSM-5	3.43	81.9	-	13.7	20.86	
NbP/HZSM-5	3.06	72.7	11.7	11.6	20.16	1.60
NbP/HZSM-5+Li	3.24	76.9	8.86	9.95	20.14	1.80

XRF analysis confirms the successful incorporation of Nb and P elements into the catalyst during stepwise modification, while the Si/Al ratio of the zeolite framework remains largely unchanged.

Table S3 Microscopic properties of catalyst

catalyst	Surface area (m^2/g)	Pore volume (cm^3/g)	Pore size (nm)
HZSM-5	315.41	0.21	4.43
Nb_2O_5/HZSM-5	292.74	0.19	3.83
NbP/HZSM-5	210.05	0.15	5.83
NbP/HZSM-5+Li	179.51	0.20	5.70

During the stepwise modification process, the specific surface area and pore structure of the catalyst undergo systematic evolution. Although phosphorylation reduces the specific surface area, it significantly increases the pore size, which is beneficial for improving the accessibility of substrate molecules to active sites and enhancing mass transfer efficiency.

Table S4 Acidic properties of catalysts

Catalyst	Weak + Moderate acidity		Strong acidity		Total acidity (mmol/g)
	T(°C)	Amount (mmol/g)	T(°C)	Amount (mmol/g)	
HZSM-5	50-500	56.34	500-700	4.92	56.34
Nb_2O_5/HZSM-5	50-500	59.06	500-700	7.03	66.09-
NbP/HZSM-5	50-500	63.48	500-700	21.13	84.61
NbP/HZSM-5+Li	50-500	89.09	500-700	7.06	96.15

The data indicate that phosphorylation significantly enhances the strong acidity of the catalyst, while Li^+ modification markedly increases the content of weak-to-moderate acid sites and reshapes the acid distribution, thereby tailoring the catalyst's acidity for improved suitability in multi-step cascade reactions.

Table S5 Contents of Lewis acid and Brønsted acid

Catalyst	B acid (μmol/g)	L acid (μmol/g)	B/L
Nb-P/HZSM-5	113.24	6.50	17.42
Nb-P/HZSM-5+Li	113.74	23.53	4.83

As evidenced by the data comparison, Li^+ modification significantly increases the Lewis acid content while maintaining the number of Brønsted acid sites largely unchanged. This transforms the acid site distribution of the catalyst from being predominantly Brønsted acidic (B/L=17.42) to a more synergistic coexistence of Brønsted and Lewis acids (B/L=4.83).

Table S6 Calculated H_0 values at 298 K

Entry	MS	A_{375nm}	[I]	$[IH^+]$	H_0
1	blank	0.955	100	0	-
2	FA+H_2O	0.933	93.4	6.6	2.13
3	LA+H_2O	0.953	99.79	0.21	3.67
4	LiCl·3H_2O	0.932	93.4	6.6	2.14
5	NbP/HZSM-5+H_2O	0.954	99.9	0.10	3.90
6	FA+LiCl·3H_2O	0.251	26.3	73.7	0.54
7	LA+LiCl·3H_2O	0.515	54.7	45.3	1.07
8	NbP/HZSM-5+LiCl·3H_2O	0.481	50.4	49.6	1.00

The data in the table show that LiCl·3H_2O significantly reduces the Hammett acidity function values of formic acid, levulinic acid, and the solid catalyst, indicating that the molten salt can effectively enhance the proton-donating capability of each acidic component.

Table S7 Cellulose dissolvability in $LiCl \cdot nH_2O$

Molar ration of H_2O/LiCl	1	1.5	2	3	4	5	6
pH	-	-	5.16	5.28	5.61	5.87	5.95
dosage，g	1.50	0.50	0.50	0.50	0.50	0.50	0.50
appearance							

Table S7 demonstrates that cellulose dissolvability in $LiCl \cdot nH_2O$ is highly dependent on the hydration number (n), with optimal disruption of the crystalline structure achieved at a specific molar ratio of H_2O to LiCl, as indicated by the changes in pH and dosage.

Table S8 Kinetic parameters for glucose conversion to LA in H_2O + NbP/HZSM-5

Entry	Temperature(°C)	K_1	K_2	K_3	K_4
1	120	1.43×10^{-4}	1.44×10^{-3}	4.94×10^{-4}	5.02×10^{-4}
2	130	3.42×10^{-4}	2.14×10^{-3}	2.84×10^{-6}	4.34×10^{-6}
3	140	3.58×10^{-3}	3.27×10^{-3}	1.09×10-3	1.02×10-1
4	150	2.52×10^{-3}	6.33×10-3	1.74×10^{-3}	1.57×10^{-2}
5	160	7.39×10^{-3}	2.22×10^{-14}	2.31×10^{-2}	2.72×10^{-2}
6	170	8.54×10^{-3}	3.23×10^{-14}	5.43×10^{-2}	2.78×10^{-2}

The data in the table show that the rate constants (K_1–K_4) for the elementary reaction steps in the conversion of glucose to LA over NbP/HZSM-5 generally increase with rising reaction temperature (120–170 °C), indicating that elevated temperature synergistically promotes the kinetics of the multi-step cascade.

1) Ea_1 and A_1 were derived from k_1 values at 150–170 °C. This was necessary because the reaction was prohibitively slow below 140 °C, resulting in immeasurably small k_1.
2) Ea_2 and A_2 were based on k_2 values at 120–150 °C. At higher temperatures, the rapid consumption of fructose led to its near-complete depletion, precluding accurate measurement.
3) Ea_3/A_3 and Ea_4/A_4 were calculated using k_3 and k_4 at 150–170 °C, as the conversion of HMF to LA was negligible below 140 °C.

Table S9 kinetic parameters for glucose conversion to LA in $LiCl{\cdot}3H_2O$ + NbP/HZSM-5

Entry	Temperature(°C)	K_1	K_2	K_3	K_4
1	120	9.13×10^{-4}	4.76×10^{-3}	2.38×10^{-2}	2.22×10^{-14}
2	130	2.16×10^{-3}	7.90×10^{-3}	1.26×10^{-2}	2.22×10^{-14}
3	140	6.61×10^{-3}	1.18×10^{-2}	1.29×10-2	1.09×10^{-2}
4	150	4.31×10^{-2}	1.30×10^{-2}	4.03×10^{-2}	2.22×10^{-3}
5	160	6.66×10^{-2}	1.15×10^{-2}	5.24×10^{-2}	2.59×10^{-3}
6	170	1.30×10^{-1}	1.92×10^{-2}	9.63×10^{-2}	2.92×10^{-3}

In the molten salt synergistic catalytic system, the rate constants for all elementary steps of glucose conversion are significantly enhanced and exhibit a coordinated increase with rising temperature, highlighting the system's overall enhancement of reaction kinetics.

1) Ea_1 and A_1 were derived from k_1 values at 140–170 °C. This was necessary because the reaction was prohibitively slow below 140 °C, resulting in immeasurably small k_1.
2) Ea_2 and A_2 were based on k_2 values at 120–140 °C. At higher temperatures, the rapid consumption of fructose led to its near-complete depletion, precluding accurate measurement.
3) Ea_3/A_3 and Ea_4/A_4 were calculated using k_3 and k_4 at 150–170 °C, as the conversion of HMF to LA was negligible below 140 °C.

Table S10 Comparison of the process greenness in different approaches for the synthesis of levulinic acid from cellulose

Entry	Reaction system, catalyst	LA yield (%)	Toxicity (GHS)	E-factor (kg waste/kg LA)	AE (%)	RE (%)	EE (mol LA/MJ)	Ref
1	aqueous, $CrCl_3$	67.0	3	4.2	45.3	42.5	0.32	[1]
2	aqueous, $RuCl_3$	87.6	3	3.8	48.1	38.2	0.35	[2]
3	[BSMim]HSO_4 (IL)	39.4	2	6.5	32.7	56.8	0.21	[3]
4	$ZnCl_2 \cdot 3H_2O$, SO_4^{2-}/TiO_2	43.1	1	5.1	38.9	61.3	0.29	[4]
5	90% GVL + 10% Water, CP-SO_3H	65.5	2	3.5	44.7	68.5	0.41	[5]
6	MIBK+NaCl aqueous, Lignin-based solid acid	60.0	2	3.5	51.2	80.0	0.58	[6]
7	aqueous, heteropoly acid/Carbon foam	58.0	1	3.2	53.6	82.0	0.63	[7]
8	MIBK+$LiCl \cdot 3H_2O$, $NbOPO_4$/HZSM-5	94.0	1	2.8	52.3	76.4	0.78	[8]
9	$LiCl \cdot 3H_2O$, NbP/HZSM-5	85.8	0	1.2	68.7	89.7	0.87	This work

AE: atom economy, %; RE: recyclability economy, %; EE: energy efficiency, mole of levulinic acid produced per million joules energy consumed, mol LA/MJ

1. Explanation of Calculation Standards and Data Consistency

1.1 All literature Entries adopted correction factors derived from the general conversion standards of *Green Chemistry* thematic issue [9] and cited literatures, ensuring data comparability across different systems.

1.2 This data in this work was not subjected to additional toxicity/loss corrections; only unit unification was performed to align results with actual reaction conditions.

1.3 The error range of ±5% (from weighing, energy consumption calculation, and correction factor selection) does not affect the relative ranking of green advantages.

1.4 All calculations followed the unified standards of *Green Chemistry* thematic issue [1] and authoritative literatures [10-11], using "0.1 g cellulose as substrate, 175℃, 2 h" as the unified benchmark (literature data were converted per original conditions). Core parameters: cellulose molar mass = 162 g/mol, LA molar mass = 116 g/mol; waste = humins + unreacted cellulose (recyclable solvents/catalysts excluded).

2. Acquisition and Determination Process of GHS Toxicity Scores

The GHS toxicity scores (0-3 points) in Table 3 are strictly derived through dual verification of "official database query + classification standard comparison" in accordance with the latest revised edition of the United Nations GHS (11th Edition, 2025) and corresponding regional regulations (such as China's GB 30000 series and the EU CLP Regulation). The specific process is as follows:

Core Determination Basis and Scoring Rules

(1) Sources of Scoring Standards

International Unified Standard: The "Guidelines for Classification of Health Hazards" (Chapters 3.1-3.10) in the *Globally Harmonized System of Classification and Labelling of Chemicals (GHS) 11th Revised Edition*, which specifies classification thresholds for 10 types of health hazards including acute toxicity, skin irritation/corrosion, and sensitization (e.g., acute oral toxicity with LD_{50} < 200 mg/kg is classified as Category 3).

Regional Regulation Adaptation: China (GB 30000.10-2024) and the EU (CLP Regulation, Regulation (EC) No 1272/2008) are referenced to ensure compliance with target market requirements.

(2) Scoring Rules

0: non-toxic, non-irritating, non-corrosive; 1: Mild health hazards; 2: Moderate health hazards; 3: Severe health hazards

3. **E-factor:** a core green chemistry metric for quantifying waste generation in catalytic processes, defined as the mass ratio of total waste (byproducts, unreacted feedstock, and residual components) to the mass of target product produced. A lower E-factor indicates more efficient waste minimization, aligning with the Green Chemistry principle of waste reduction.
4. **Atom Economy (AE)**: Molar mass ratio of LA to the total molar mass of reactants (excluding recyclable components), with a correction factor for activity loss, solvent recovery, and impurity content.
5. **Recyclability Efficiency (RE)**: Percentage of catalyst and solvent recovered after four cycles, weighted by their retained activity.
6. **Energy Efficiency (EE)**: LA yield per unit energy input, calculated as mol LA/MJ (moles of LA produced per million joules of energy consumed).

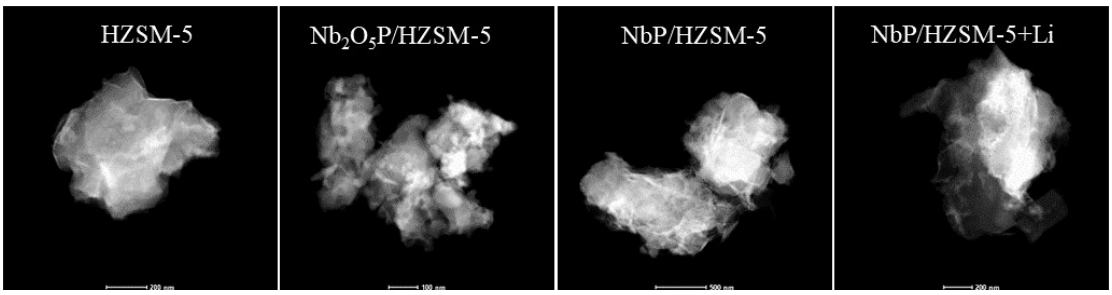

Fig. S1 TEM images of HZSM-5, Nb/HZSM-5, NbP/HZSM-5 and NbP/HZSM-5+Li

TEM images reveal that phosphorylation transforms the catalyst into a hierarchical flower-like superstructure, while subsequent Li^+ modification maintains this morphology and further promotes the uniform dispersion of the active phase.

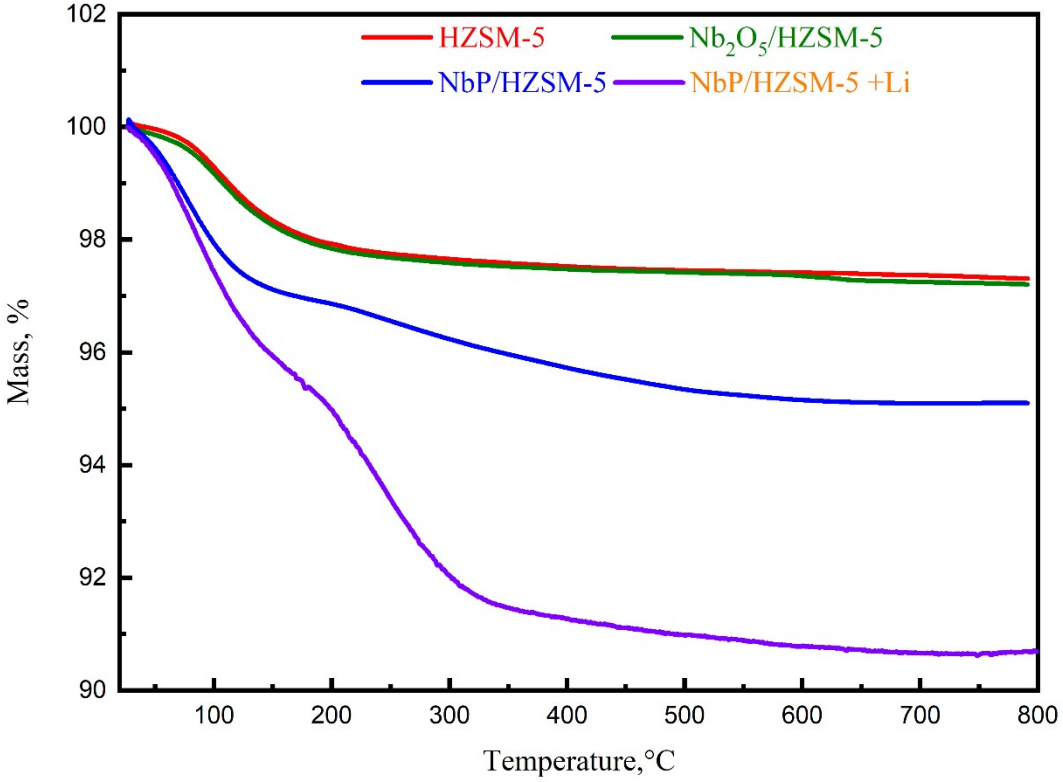

Fig. S2 Thermal gravimetric curves of various catalysts

The TGA curves indicate that phosphorylation and subsequent Li^+ modification significantly alter the low-temperature mass loss behavior of the catalysts, reflecting tailored surface hydration and thermal stability.

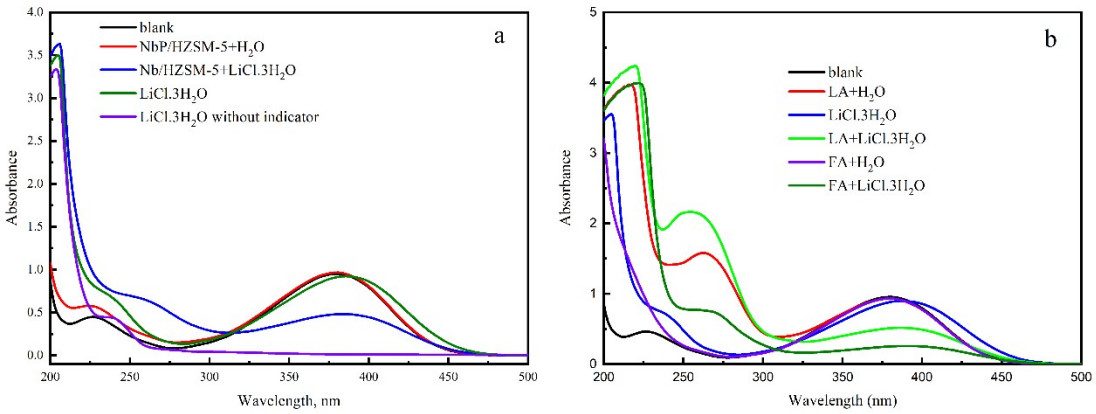

Fig. S3 UV-vis spectra of various samples in the presence of 4-nitroaniline as an indicator

The UV-Vis spectra, obtained using 4-nitroaniline as a Hammett indicator, characterize the acidic strength of various samples. [12] The shift in the absorption peak of the indicator across different curves visually reflects differences in system acidity, with the molten salt hydrate environment notably enhancing the proton-donating capability of the acid sites.

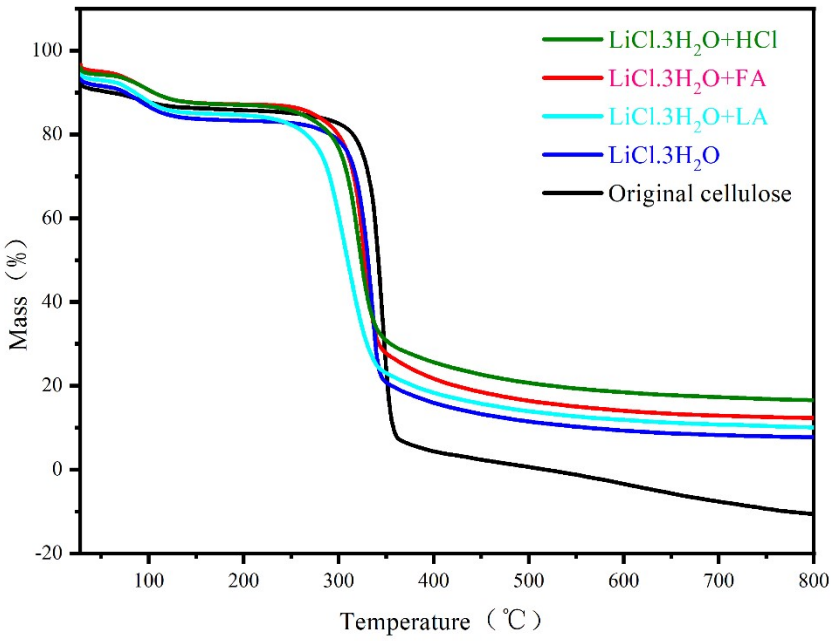

Fig. S4 Thermal gravimetric curves of (a) original cellulose and (b) Regenerated Cellulose

The reduced thermal stability of regenerated cellulose signals extensive crystalline disruption. The resulting amorphous structure promotes substrate accessibility to active sites in the catalytic system, thus enhancing the efficiency of the subsequent conversion cascade.

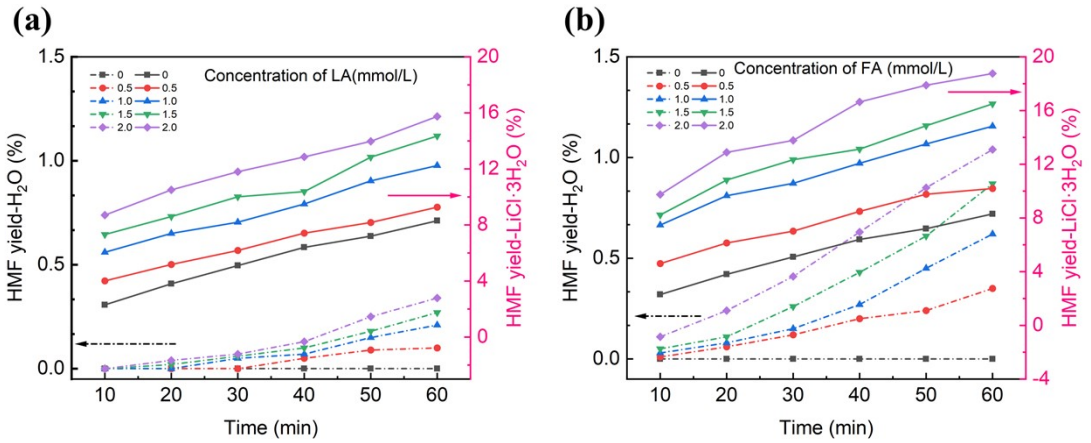

Fig. S5 Effect of FA and LA concentrations on cellulose conversion (a) LA; (b) FA
Conditions:0.6 g MCC, 30 mL H_2O or $LiCl·3H_2O$, 150°C

LA and FA significantly accelerate HMF formation, especially in $LiCl·3H_2O$ which confirms that in situ-generated acids create an "autocatalytic proton shuttle" via a dynamic proton transfer network.

Reference

[1] L. Peng, L. Lin, J. Zhang, J. Zhuang, B. Zhang, Y. Gong, Molecules, 2010, 15, 8, 5258-5272.

[2] L. Yan, R. Ma, H. Wei, L. Li, B. Zou, Y. Xu, Bioresour. Technol., 2019, 279, 84-91.

[3] Y. Shen, J. K. Sun, Y. X. Yi, B. Wang, F. Xu, R. C. Sun, Bioresour. Technol., 2015, 192, 812-816.

[4] W. Wei, S. Wu, Bioresour. Technol., 2017, 241, 760-766.

[5] 61 Y. Zuo, Y. Zhang, Y. Fu. ChemCatChem, 2014, 6, 3, 753-757

[6] Z. Chen, S. Zhang, B.o Yan, Q. Cai, S. Zhang, Ind. Crops Prod., 2022, 178. 114523

[7] X. Xu, B. Liang, Y. Zhu, J. Chen, T. Gan, H. Hu, Y. Zhang, Z. Huang, Y. Qin, Bioresour. Technol., 2023, 387, 129600

[8] J. Wang, H. Cui, Y. Wang, R. Zhao, Y. Xie, M. Wang, W. Yi, *Green Chem.,* 2020, 22, 4240-4251

[9] A. Bardow, J. Pérez-Ramírez, S. Sala, L. Vaccaro, *Green Chem*., 2024, 26, 11016-11018.

[10] E. Lucas, A. J. Martín, S. Mitchell, A. Nabera, L. F. Santos, J., Pérez-Ramírez, G. Guillén-Gosálbez, *Green Chem.* 2024, **26,** 9300-9309.

[11] P. M., Nowak, *Green Chem.*, 2023, **25,** 4625-4640.

[12] J. Wang, H. Cui, J. Wang, Z. Li, M. Wang, W. Yi, *Appl. Catal. A-Gen.*, 2022, **638**, 118640.